drones

Article

Prescribed Performance Fault-Tolerant Attitude Tracking Control for UAV with Actuator Faults

Qilong Wu and Qidan Zhu *

College of Intelligent Systems Science and Engineering, Harbin Engineering University, Harbin 150001, China; wuqilong@hrbeu.edu.cn
* Correspondence: zhuqidan@hrbeu.edu.cn

Abstract: This paper proposes a prescribed performance fault-tolerant control based on a fixed-time extended state observer (FXTESO) for a carrier-based unmanned aerial vehicle (UAV). First, the attitude motion model of the UAV is introduced. Secondly, the proposed FXTESO is designed to estimate the total disturbances including coupling, actuator faults and external disturbances. By using the barrier Lyapunov function (BLF), it is proved that under prescribed performance control (PPC), the attitude tracking error is stable within the prescribed range. The simulation results for tracking the desired attitude angle show that the average overshoot and stabilization time of PPC-FXTESO is 0.00455 rad and 6.2 s. Comparatively, the average overshoots of BSC-ESO and BSC-FTESO are 0.035 rad and 0.027 rad, with stabilization times of 14.97 s and 12.56 s, respectively. Therefore, the control scheme proposed in this paper outperforms other control schemes.

Keywords: carrier-based unmanned aerial vehicle; attitude control; fixed-time extended state observer; barrier Lyapunov function

check for updates

Citation: Wu, Q.; Zhu, Q. Prescribed Performance Fault-Tolerant Attitude Tracking Control for UAV with Actuator Faults. *Drones* **2024**, *8*, 204. https://doi.org/10.3390/drones8050204

Academic Editor: Abdessattar Abdelkefi

Received: 30 March 2024
Revised: 11 May 2024
Accepted: 15 May 2024
Published: 16 May 2024

1. Introduction

The carrier-based UAV attitude tracking control plays a role in the automatic landing process, and a stable flight attitude can ensure the safety of the aircraft-landing process. The UAV may encounter actuator faults and external disturbances during attitude tracking, and these disturbances can also seriously affect the landing accuracy. Ensuring the aircraft can track the desired attitude accurately and rapidly during actuator faults is crucial for the automatic carrier landing system. Actuator faults are one of the most common faults during flight, and in order to improve the safety and reliability of the system, fault tolerance will also be an issue to be considered [1].

The fault-tolerant control methods can be categorized into two main groups: active fault tolerance and passive fault tolerance. Passive fault tolerance is primarily based on the design concept of robust control, utilizing a fixed controller structure for a specific fault type. To address the issue of commercial aircraft being affected by actuator faults during longitudinal motion, reference [2] proposes an adaptive control scheme. The actuator faults can be estimated online by adaptive control [3]. However, the passive fault-tolerant control method has limited fault-tolerant capability, and the performance of the system will not be guaranteed when the type or degree of fault exceeds a predetermined range. Active fault tolerance is mainly based on the system's fault information to actively reconfigure the model or controller. Reference [4] designs an active fault-tolerant control that is robust to potential undetected actuator faults. Advanced control schemes must be introduced to enhance the fault-tolerant control capability of the attitude control system.

Attitude controller designs employ a variety of intelligent control methods, including backstepping control [5–7], sliding mode control [8,9], active disturbance rejection control (ADRC) [10], and model predictive control [11]. Among them, backstepping techniques can reduce the complexity of higher-order systems by iterative design, and thus have been widely used. The sliding mode control is used for aircraft attitude fault-tolerant control systems [9]. However, the chattering phenomenon affects the application of sliding mode control in aircraft attitude tracking systems. The adaptive control strategy enables the attitude system to track the desired angle when the actuator fails [12,13]. However, when the system changes rapidly, the performance of adaptive controllers decreases. The aforementioned sliding mode control and adaptive control schemes can improve the robustness of the attitude control system but may degrade the control performance. References [14,15] proposes fault estimation observers for estimating actuator faults. Therefore, control based on the extended state observer (ESO) is proposed for application to the attitude tracking control problem [16]. The ESO considers the actuator faults, channel coupling and external disturbances of the system as total perturbations, and estimates and compensates the total perturbations [17–20]. However, the studies above can only ensure asymptotic convergence and infinite convergence time. The fixed-time theory ensures that the upper bound stability time remains a fixed value irrespective of the system's initial state [21], thereby introducing systems with fixed-time convergence [22,23]. Furthermore, in [24], a novel fixed-time convergence system is proposed, achieving faster convergence. The finite time extended state observer combines finite time control and extended state observer [25], which can accurately estimate the total disturbances within a finite time. The simulation comparison shows that the proposed FXTESO is more accurate in estimating the total disturbances and has a faster convergence speed.

In the above results, the system state is not constrained. Since the prescribed performance control (PPC) method can control the transient performance and steady-state performance of the system [26], it is used in many fields, such as spacecraft attitude systems [27], unmanned surface vehicles [28], automatic carrier landing [29]. The control framework combining the barrier Lyapunov function (BLF) method and PPC has been widely used [30,31]. The BLF is proposed in [32] for the controller design of nonlinear systems with static output constraints. In [33], an output constraint controller based on neural networks is proposed, in which the barrier Lyapunov function is used to ensure system state constraints. In order to achieve the specified output tracking performance, a backstepping controller based on the PPC method is used to control the spacecraft attitude tracking in [34]. Reference [35] proposes an MPC-based fault detection and diagnosis (FDD) and fault-tolerant control (FTC) strategy to mitigate the effects of faults. The solution is robust to uncertainties and disturbances in the model. In contrast, prescribed performance control based on a fixed-time extended state observer does not involve a complex optimization process and therefore better meets the real-time requirements. It relies mainly on the extended state observer to estimate the system state, thus not requiring rigorous system modeling.

Many scholars have studied the control of the carrier-based UAV. Reference [36] utilizes RBFNN to estimate the perturbations in the attitude control system of a carrier-based aircraft and designs a second-order sliding mode controller to ensure the stability of the attitude control system within a finite time. Reference [37] addresses the resource allocation problem for the UAV. Reference [38] proposes robust optimal tracking control to minimize the cost function while handling uncertainty and stabilizing the closed-loop system. For robust longitudinal fault-tolerant control of the carrier-based UAV, reference [39] proposes a control scheme that combines state observer, adaptive control, and backstepping control, which allows the UAV to achieve more stable longitudinal trajectory tracking control under actuator failure. The adaptive neural network method is proposed to compensate for the faulty term during the tracking of the desired glide path of the carrier-based UAV, combined with a sliding mode control method so that the aircraft can safely land on the carrier [40]. An adaptive fault-tolerant control method is proposed for handling actuator failures during the tracking of the desired glide path by the carrier-based aircraft. Comparative results show that the improved robust adaptive fault-tolerant control can effectively handle both parametric and nonparametric faults as well as external disturbances [41]. Compensation for faults and uncertainty terms in the carrier-based UAV is made using adaptive prescribed performance control methods [42]. The controller ensures that the stability performance and transient performance of the carrier-based UAV tracking error are within the preset range. Simulation results show that the proposed controller can accurately track the desired value under external disturbance while satisfying the prescribed performance requirements.

This work proposes a fixed-time extended state observer-based prescribed performance approach that is applied to the UAV attitude control system based on the above discussion. The primary contributions are as follows:

(1) A fixed-time extended state observer is utilized to estimate the model's external perturbations and actuator faults. Different from traditional ESO and FTESO, the FXTESO proposed in this paper achieves fixed-time stability, and the convergence time is independent of the initial conditions.

(2) The proposed control scheme ensures that the carrier-based UAV tracks the desired attitude angle according to the prescribed performance requirements. The controller design considers the PPC constraints on attitude tracking errors and combines the PPC with the BLF to achieve the desired attitude tracking control objectives.

This paper is organized as follows: The carrier-based UAV attitude dynamics model with actuator failures is described in Section 2. Section 3 designs the PPC-FXTESO, and Section 4 applies the control method to the attitude control system. The simulation results demonstrate the control method's efficacy, and Section 5 presents the conclusion.

2. Problem Formulation

This section describes a dynamic model of the UAV with external disturbances. According to [43], actuators include an elevator (δ_e), aileron (δ_a), and rudder (δ_r). As shown in the Figure 1 body coordinate system $Ox_by_bz_b$ (denoted as S_b), on an aircraft, the center of mass is generally taken as the origin; axis x_b is parallel to the longitudinal symmetry axis of the fuselage and points to the direction of the nose; axis y_b is perpendicular to x_b and points to the right; and the z_b axis is perpendicular to the Ox_by_b plane along the origin, and the direction is downward. The ground coordinate system $Ox_gy_gz_g$ (denoted as S_g) is located on the Earth's surface. The origin O can be chosen arbitrarily on the ground, where the direction of the x_g axis is arbitrary and is on the ground plane; the z_g axis is vertical downward; the right-hand criterion determines the y_g axis. Three attitude angles can be used to convert between the ground and body coordinate systems. The definitions of each angle are as follows: Pitch angle θ represents the pitch attitude of the aircraft, usually calibrated using the angle between the body axis Ox_b and its projection on the plane Ox_gy_g, and the aircraft θ is positive when looking up and negative when looking down. Roll angle ϕ is the angle formed by the aircraft system plane Ox_bz_b and the geodetic coordinate system plane Ox_gz_g; viewed along the flight direction, ϕ is positive when the right wing of the aircraft descends, and is negative when the left wing descends. Yaw angle ψ is the angle made by the projection of the longitudinal axis Ox_b of the body coordinate system onto the plane of the geodetic coordinate system Ox_gy_g concerning the axis Ox_g; ψ is positive when the projection is on the right side of the Ox_g axis and negative when it is on the left side.

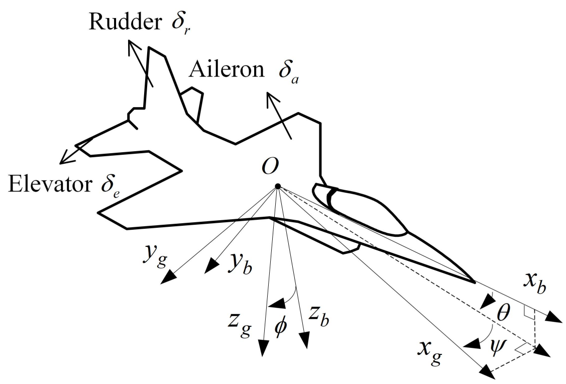

Figure 1. Aircraft actuators and attitude angles.

2.1. Model of the UAV

The attitude dynamics model of a fixed-wing UAV can be written as [36]:

$$\begin{cases} \dot{\phi} = p + r\cos\phi\tan\theta + q\sin\phi\tan\theta \\ \dot{\theta} = q\cos\phi - r\sin\phi \\ \dot{\psi} = r\sec\theta\cos\phi + q\sec\theta\sin\phi \\ \dot{p} = (a_1 r + a_2 p)q + a_3 L + a_4 N \\ \dot{q} = a_5 pr - a_6\left(p^2 - r^2\right) + a_7 M \\ \dot{r} = (a_8 p - a_2 r)q + a_4 L + a_9 N \end{cases} \tag{1}$$

where $a_1 = \left(J_y - J_z\right)J_z - J_{xz}^2/\Sigma, a_2 = \left(J_x - J_y + J_z\right)J_{xz}/\Sigma, a_3 = J_z/\Sigma, a_4 = J_{xz}/\Sigma,$ $a_5 = J_z - J_x/J_y, a_6 = J_{xz}/J_y, a_7 = 1/J_y, a_8 = J_x\left(J_x - J_y\right) + J_{xz}^2/\Sigma, a_9 = J_x/\Sigma, \Sigma = J_x J_z - J_{xz}^2.$

The aerodynamic moments can be defined as:

$$\begin{bmatrix} L \\ M \\ N \end{bmatrix} = \mathrm{QS}\begin{bmatrix} b\left(C_{l\beta}\beta + C_{lp}\frac{pb}{2V} + C_{lr}\frac{rb}{2V} + C_{l\delta_a}\delta_a + C_{l\delta_r}\delta_r\right) \\ c\left(C_{m0} + C_{m\alpha}\alpha + C_{mq}\frac{qc}{2V} + C_{m\delta_e}\delta_e\right) \\ b\left(C_{n\beta}\beta + C_{np}\frac{pb}{2V} + C_{nr}\frac{rb}{2V} + C_{n\delta_a}\delta_a + C_{n\delta_r}\delta_r\right) \end{bmatrix} \tag{2}$$

where L, M, and N represent the aerodynamic moments of roll, pitch, and yaw, respectively. $C_{l\beta}, C_{lp}, C_{lr}, C_{l\delta_a}, C_{l\delta_r}$ are rolling moment coefficients, $C_{m0}, C_{m\alpha}, C_{mq}, C_{m\delta_e}$ are pitching moment coefficients, $C_{n\beta}, C_{np}, C_{nr}, C_{n\delta_a}, C_{n\delta_r}$ are yawing moment coefficients, $Q = \rho V^2/2$, V denotes the velocity of the aircraft, α is the angle of attack, β is the sideslip angle, and ρ is air density.

The following affine nonlinear form:

$$\begin{cases} \dot{\boldsymbol{\Omega}} = \boldsymbol{R}(\boldsymbol{\Omega})\boldsymbol{\omega} \\ \dot{\boldsymbol{\omega}} = \boldsymbol{f}_\omega + \boldsymbol{g}_\omega\left(\boldsymbol{u} + \boldsymbol{u}_f\right) + \boldsymbol{d}_\omega \end{cases} \tag{3}$$

where $\boldsymbol{\Omega} = [\phi, \theta, \psi]^{\mathrm{T}}$ denote the angle, $\boldsymbol{\omega} = [p, q, r]^{\mathrm{T}}$ denote the angular rate, and $\boldsymbol{u} = [\delta_a, \delta_e, \delta_r]^{\mathrm{T}}$. $\boldsymbol{d}_\omega = [d_1, d_2, d_3]^{\mathrm{T}}$ is the external disturbance vector; $\boldsymbol{u}_f = \left[u_{f1}, u_{f2}, u_{f3}\right]^{\mathrm{T}}$ is the actuator faults vector; and $\boldsymbol{R}(\boldsymbol{\Omega}), \boldsymbol{f}_\omega, \boldsymbol{g}_\omega$ are defined as

$$\boldsymbol{R}(\boldsymbol{\Omega}) = \begin{bmatrix} 1 & \sin\phi\tan\theta & \cos\phi\tan\theta \\ 0 & \cos\phi & -\sin\phi \\ 0 & \sin\phi\sec\theta & \cos\phi\sec\theta \end{bmatrix} \tag{4}$$

$$\boldsymbol{f}_\omega = \begin{bmatrix} \begin{pmatrix} a_1 qr + a_2 pq + a_3 Qb\Big(C_{l\beta}\beta + C_{lp}bp/2V \\ +C_{lr}br/2V\Big) \\ +a_4 Qb\left(C_{n\beta}\beta + C_{np}bp/2V + C_{nr}br/2V\right) \end{pmatrix} \\ \left(a_5 pr + a_6\left(r^2 - p^2\right) + a_7 Qc\left(C_{m0} + C_{m\alpha}\alpha \right.\right. \\ \left.\left. +C_{mq}cq/2V\right)\right) \\ \begin{pmatrix} -a_2 qr + a_8 pq + a_4 Qb\Big(C_{l\beta}\beta + C_{lp}bp/2V \\ +C_{lr}br/2V\Big) \\ +a_9 Qb\left(C_{n\beta}\beta + C_{np}bp/2V + C_{nr}br/2V\right) \end{pmatrix} \end{bmatrix} \tag{5}$$

$$\boldsymbol{g}_\omega = \begin{bmatrix} Qb\left(a_3 C_{l\delta_a} + a_4 C_{n\delta_a}\right) & 0 & Qb\left(a_3 C_{l\delta_r} + a_4 C_{n\delta_r}\right) \\ 0 & a_7 QcC_{m\delta_e} & 0 \\ Qb\left(a_4 C_{l\delta_a} + a_9 C_{n\delta_a}\right) & 0 & Qb\left(a_4 C_{l\delta_r} + a_9 C_{n\delta_r}\right) \end{bmatrix} \tag{6}$$

2.2. Actuator Faults

The actuator has a vital role in the various components of the flight control system. Actuator failure characteristics can be divided into four types: jamming, random drift, saturation, and partial damage. This paper focuses on studying actuator drift faults:

$$\boldsymbol{u}_f = \begin{bmatrix} u_{f1} \\ u_{f2} \\ u_{f3} \end{bmatrix} = \begin{bmatrix} 0.5\sin(2t) + 0.5 \\ 7 \\ 0.5\sin(t) + 0.5 \end{bmatrix} \tag{7}$$

Actuator faults occur when $t \geq 10$ s. Time-varying faults can be caused by the gradual failure of certain components in an actuator over time. Constant faults are fixed failures of some components or parts in the actuator that do not change over time.

3. Carrier-Based UAV Attitude Controller Design

A prescribed performance fault-tolerant attitude tracking controller based on FXTESO is proposed for the carrier-based UAV attitude system. The proposed controller enables the UAV to maintain good attitude tracking performance even when the actuator fails. Figure 2 shows the design of the attitude tracking control system with actuator faults. This paper designs a prescribed performance fault-tolerant controller for the inner and outer loop of the attitude control system. In addition, the FXTESO scheme is proposed to estimate the total disturbances.

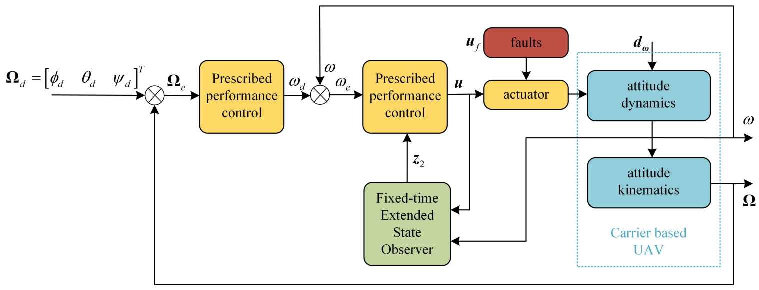

Figure 2. Diagram of the carrier-based UAV attitude control system based on PPC-FXTESO.

3.1. FXTESO Design

The extended state observer has a strong estimation capability, first proposed by Han [44]. The extended state observer can estimate the state quantities of the system and the external disturbances of the controlled object according to the inputs and outputs of the system, and can be detached from the controlled system and the external dynamic model. A controller can be designed to compensate for the estimated external disturbances. The design of the FXTESO is as follows.

Lemma 1 ([45])**.** *For any $\boldsymbol{x} \in \mathbb{R}^3$ and $\boldsymbol{y} > 0$, if $|\boldsymbol{x}| < \boldsymbol{y}$, then it holds that*

$$\ln\left[\boldsymbol{y}^2 / \left(\boldsymbol{y}^2 - \boldsymbol{x}^2\right)\right] \leq \boldsymbol{x}^2 / \left(\boldsymbol{y}^2 - \boldsymbol{x}^2\right) \tag{8}$$

Lemma 2 ([46])**.** *V is positive definite, and then there also exist real number d and θ satisfying $d > 0$ and $\theta \in (0,1)$ such that $\dot{V}(x) + d(V(t))^{\theta} \leq 0$. Then, the settling time T satisfies*

$$T \leq \frac{1}{d(1-\theta)}(V(x))^{(1-\theta)}$$

The extended system state $\boldsymbol{x_1} = \boldsymbol{\omega}, \boldsymbol{x_2} = \boldsymbol{f_\omega} + \boldsymbol{g_\omega u_f} + \boldsymbol{d_\omega} = \boldsymbol{F_\omega}$ in Equation (3) can be established as

$$\begin{cases} \dot{\boldsymbol{x}}_1 = \boldsymbol{g_\omega u} + \boldsymbol{x}_2 \\ \dot{\boldsymbol{x}}_2 = \dot{\boldsymbol{F}}_\omega \end{cases} \tag{9}$$

Therefore, the FXTESO can be constructed as

$$\begin{cases} \boldsymbol{e}_1 = \boldsymbol{z}_1 - \boldsymbol{x}_1 \\ \dot{\boldsymbol{z}}_1 = \boldsymbol{z}_2 - \lambda_1 sig^{a_1}(\boldsymbol{e}_1) - k_1 sig^{b_1}(\boldsymbol{e}_1) + \boldsymbol{g}_\omega \boldsymbol{u} \\ \dot{\boldsymbol{z}}_2 = -\lambda_2 sig^{a_2}(\boldsymbol{e}_1) - k_2 sig^{b_2}(\boldsymbol{e}_1) + Ksgn(\boldsymbol{e}_1) \end{cases} \tag{10}$$

where $\mathrm{sig}^{a_1}(e_1) = \mathrm{sgn}(e_1) \cdot |e_1|^{a_1}, a_i \in (0,1), b_i > 1, i = 1,2$ and satisfy $a_1 = a, a_2 = 2a-1$, $b_1 = b, b_2 = 2b-1$. Increasing the gain of the FXTESO can accelerate the convergence speed, but excessively large parameters may lead to observer chattering. Therefore, it is necessary to select smaller parameters for the FXTESO to maintain satisfactory convergence speed.

The following FXTESO estimation error

$$\begin{cases} \dot{\boldsymbol{e}}_1 = \boldsymbol{e}_2 - \lambda_1 sig^{a_1}(\boldsymbol{e}_1) - k_1 sig^{b_1}(\boldsymbol{e}_1) \\ \dot{\boldsymbol{e}}_2 = -\lambda_2 sig^{a_2}(\boldsymbol{e}_1) - k_2 sig^{b_2}(\boldsymbol{e}_1) + Ksgn(\boldsymbol{e}_1) - \dot{\boldsymbol{F}}_\omega \end{cases} \tag{11}$$

where $\boldsymbol{e}_i = \boldsymbol{z}_i - \boldsymbol{x}_i, (i = 1,2)$ is the estimation error of the fixed-time extended state observer.

Theorem 1. *In any initial state, Equation (10) can estimate the state variable in a fixed time, and the estimation error will converge to a small range in a fixed time.*

The following error formula

$$\begin{cases} \dot{\boldsymbol{e}}_1 = \boldsymbol{e}_2 - \lambda_1 sig^{a_1}(\boldsymbol{e}_1) - k_1 sig^{b_1}(\boldsymbol{e}_1) \\ \dot{\boldsymbol{e}}_2 = -\lambda_2 sig^{a_2}(\boldsymbol{e}_1) - k_2 sig^{b_2}(\boldsymbol{e}_1) \end{cases} \tag{12}$$

Define $\boldsymbol{e} = [\boldsymbol{e}_1, \boldsymbol{e}_2]^{\mathrm{T}}$, then there exist symmetric positive definite matrix $\boldsymbol{Q}_1, \boldsymbol{Q}_2, \boldsymbol{P}_1$, and $\boldsymbol{P}_2$ such that

$$\begin{aligned} \boldsymbol{P}_1 \boldsymbol{A}_1 + \boldsymbol{A}_1^T \boldsymbol{P}_1 &= -\boldsymbol{Q}_1, \\ \boldsymbol{P}_2 \boldsymbol{A}_2 + \boldsymbol{A}_2^T \boldsymbol{P}_2 &= -\boldsymbol{Q}_2 \end{aligned} \tag{13}$$

where

$$\boldsymbol{A}_1 = \begin{bmatrix} -\lambda_1 & 1 \\ -\lambda_2 & 0 \end{bmatrix}, \quad \boldsymbol{A}_2 = \begin{bmatrix} -k_1 & 1 \\ -k_2 & 0 \end{bmatrix} \tag{14}$$

Let $V_i(\boldsymbol{e}(t)) = \boldsymbol{e}^{\mathrm{T}} \boldsymbol{P}_i \boldsymbol{e}$ be a Lyapunov function for $\dot{\boldsymbol{e}}(t) = \boldsymbol{A}_i \boldsymbol{e}(t)$, then

$$\begin{aligned} \dot{V}_1(\boldsymbol{e}(t)) &= \dot{\boldsymbol{e}}^{\mathrm{T}} \boldsymbol{P}_1 \boldsymbol{e} + \boldsymbol{e}^{\mathrm{T}} \boldsymbol{P}_1 \dot{\boldsymbol{e}} = \boldsymbol{e}^{\mathrm{T}} \left(\boldsymbol{P}_1 \boldsymbol{A}_1 + \boldsymbol{A}_1^T \boldsymbol{P}_1 \right) \boldsymbol{e} \\ &= -\boldsymbol{e}^{\mathrm{T}} \boldsymbol{Q}_1 \boldsymbol{e} < 0 \end{aligned} \tag{15}$$

$$\begin{aligned} \dot{V}_2(\boldsymbol{e}(t)) &= \dot{\boldsymbol{e}}^{\mathrm{T}} \boldsymbol{P}_2 \boldsymbol{e} + \boldsymbol{e}^{\mathrm{T}} \boldsymbol{P}_2 \dot{\boldsymbol{e}} = \boldsymbol{e}^{\mathrm{T}} \left(\boldsymbol{P}_2 \boldsymbol{A}_2 + \boldsymbol{A}_2^T \boldsymbol{P}_2 \right) \boldsymbol{e} \\ &= -\boldsymbol{e}^{\mathrm{T}} \boldsymbol{Q}_2 \boldsymbol{e} < 0 \end{aligned} \tag{16}$$

Thus, define $\zeta = \left[e_1^{1/a_1}, e_2^{1/a_2} \right]^{\mathrm{T}}$. $\dot{V}_1(\zeta)$ and $\dot{V}_2(\zeta)$ satisfy

$$\dot{V}_1(\zeta) \le -\frac{\lambda_{\min}(\boldsymbol{Q}_1)}{\lambda_{\max}(\boldsymbol{A}_1)} V_1^a(\zeta)$$

$$\dot{V}_2(\zeta) \le -\frac{\lambda_{\min}(\boldsymbol{Q}_2)}{\lambda_{\max}(\boldsymbol{A}_2)} V_2^b(\zeta)$$

where $\lambda_{\min}(Q_i) > 0$ is the minimum eigenvalue of the matrix Q_i and $\lambda_{\max}(\boldsymbol{A}_i) > 0$ is the maximum eigenvalue of the matrix $\boldsymbol{A}_i$.

According to Lemma 2, the error vector can converge to the origin in fixed time [47]:

$$T_1 \le \frac{\lambda_{\max}^{\vartheta}(A_1)}{\gamma_1 \vartheta} + \frac{1}{\gamma_2 \sigma \Delta^\sigma} \tag{17}$$

where $\gamma_1 = \lambda_{\min}(\boldsymbol{Q}_1)/\lambda_{\max}(\boldsymbol{A}_1), \gamma_2 = \lambda_{\min}(\boldsymbol{Q}_2)/\lambda_{\max}(\boldsymbol{A}_2), \vartheta = 1 - a$, $\sigma = b - 1$. *The positive constant* $\Delta \leq \lambda_{\min}(\boldsymbol{A}_2)$.

The following equation holds:

$$\dot{\boldsymbol{e}}_2 = K\,\mathrm{sgn}(\boldsymbol{e}_1) - \dot{\boldsymbol{F}}_{\boldsymbol{\omega}} = 0, t \geq T_1 \tag{18}$$

Due to the $\dot{F}_\omega$ *effect,* $\left|\dot{\boldsymbol{F}}_{\boldsymbol{\omega}}\right| < H$ *is satisfied.* $\boldsymbol{e}_2$ *will arrive at the region* $\boldsymbol{e}_2|_\tau$ *at the following time:*

$$T_2 \leq \frac{\boldsymbol{e}_2|_\tau}{K - H} \tag{19}$$

The FXTESO convergence time is as follows:

$$T = T_1 + T_2 \tag{20}$$

Theorem 1 is proved.

Remark 1. *Compared with a finite-time extended state observer (FTESO), the proposed FXTESO is more accurate in estimating the total disturbances and has a faster convergence speed.*

3.2. FXTESO-Based Prescribed Performance Controller Design for Attitude System

The controller based on PPC can ensure that the system state remains stable within the preset range only when the external interference and actuator failure are known in advance. However, since specific information about external interference and actuator failure is difficult to ascertain in advance, the idea of combining FXTESO with PPC emerged.

The prescribed performance function is defined as

$$\rho_i = (\rho_{i0} - \rho_{i\infty})\mathrm{e}^{-l_i t} + \rho_{i\infty} \tag{21}$$

The parameters ρ_{i0}, $\rho_{i\infty}$ of the prescribed performance function are chosen based on the initial value of the attitude tracking error and the steady state error. To guarantee the prescribed tracking performance $\|\boldsymbol{\Omega}_\mathrm{e} = \boldsymbol{\Omega} - \boldsymbol{\Omega}_\mathbf{d}\| < \rho_1$, the following BLF is introduced

$$V_1 = \frac{1}{2}\ln\frac{\rho_1^2}{\rho_1^2 - \boldsymbol{\Omega}_\mathrm{e}^\mathrm{T}\boldsymbol{\Omega}_\mathrm{e}}. \tag{22}$$

The time derivative of V_1 is obtained as

$$\begin{aligned}\dot{V}_1 &= \frac{1}{2}\frac{\rho_1^2 - \boldsymbol{\Omega}_\mathrm{e}^\mathrm{T}\boldsymbol{\Omega}_\mathrm{e}}{\rho_1^2}\frac{2\rho_1\dot{\rho}_1\left(\rho_1^2 - \boldsymbol{\Omega}_\mathrm{e}^\mathrm{T}\boldsymbol{\Omega}_\mathrm{e}\right) - \rho_1^2\left(2\rho_1\dot{\rho}_1 - 2\boldsymbol{\Omega}_\mathrm{e}^\mathrm{T}\dot{\boldsymbol{\Omega}}_\mathrm{e}\right)}{\left(\rho_1^2 - \boldsymbol{\Omega}_\mathrm{e}^\mathrm{T}\boldsymbol{\Omega}_\mathrm{e}\right)^2} \\ &= \frac{-\dot{\rho}_1\boldsymbol{\Omega}_\mathrm{e}^\mathrm{T}\boldsymbol{\Omega}_\mathrm{e} + \rho_1\boldsymbol{\Omega}_\mathrm{e}^\mathrm{T}\dot{\boldsymbol{\Omega}}_\mathrm{e}}{\rho_1\left(\rho_1^2 - \boldsymbol{\Omega}_\mathrm{e}^\mathrm{T}\boldsymbol{\Omega}_\mathrm{e}\right)}\end{aligned} \tag{23}$$

Substituting (3) into (23) yields

$$\begin{aligned}\dot{V}_1 &= \frac{1}{\rho_1^2 - \boldsymbol{\Omega}_\mathrm{e}^\mathrm{T}\boldsymbol{\Omega}_\mathrm{e}}\left(-\frac{\dot{\rho}_1}{\rho_1}\boldsymbol{\Omega}_\mathrm{e}^\mathrm{T}\boldsymbol{\Omega}_\mathrm{e} + \boldsymbol{\Omega}_\mathrm{e}^\mathrm{T}\dot{\boldsymbol{\Omega}}_\mathrm{e}\right) \\ &= \frac{1}{\rho_1^2 - \boldsymbol{\Omega}_\mathrm{e}^\mathrm{T}\boldsymbol{\Omega}_\mathrm{e}}\left(-\frac{\dot{\rho}_1}{\rho_1}\boldsymbol{\Omega}_\mathrm{e}^\mathrm{T}\boldsymbol{\Omega}_\mathrm{e} + \boldsymbol{\Omega}_\mathrm{e}^\mathrm{T}\left(\dot{\boldsymbol{\Omega}} - \dot{\boldsymbol{\Omega}}_\mathrm{d}\right)\right) \\ &= \frac{1}{\rho_1^2 - \boldsymbol{\Omega}_\mathrm{e}^\mathrm{T}\boldsymbol{\Omega}_\mathrm{e}}\left(-\frac{\dot{\rho}_1}{\rho_1}\boldsymbol{\Omega}_\mathrm{e}^\mathrm{T}\boldsymbol{\Omega}_\mathrm{e} + \Omega_\mathrm{e}^\mathrm{T}\left(R(\boldsymbol{\Omega})\boldsymbol{\omega} - \dot{\boldsymbol{\Omega}}_\mathrm{d}\right)\right)\end{aligned} \tag{24}$$

The virtual control $\boldsymbol{\omega}_d$ is derived as

$$\boldsymbol{\omega}_d = R^{-1}(\boldsymbol{\Omega})(\dot{\boldsymbol{\Omega}}_{\mathrm{d}} + \frac{\dot{\rho}_1}{\rho_1}\boldsymbol{\Omega}_{\mathrm{e}} - K_1\boldsymbol{\Omega}_{\mathrm{e}}) \tag{25}$$

The tracking error $\boldsymbol{\omega}_e$ is expressed as

$$\boldsymbol{\omega}_e = \boldsymbol{\omega} - \boldsymbol{\omega}_d \tag{26}$$

In order to ensure that $\|\boldsymbol{\omega}_{\mathrm{e}} = \boldsymbol{\omega} - \boldsymbol{\omega}_{\mathbf{d}}\| < \rho_2$, the following BLF is designed:

$$V_2 = V_1 + \frac{1}{2}\ln\frac{\rho_2^2}{\rho_2^2 - \boldsymbol{\omega}_e^{\mathrm{T}}\boldsymbol{\omega}_e} \tag{27}$$

Taking the time derivative of V_2, we have

$$\begin{aligned} \dot{V}_2 &= \dot{V}_1 + \frac{1}{2}\frac{\rho_2^2 - \boldsymbol{\omega}_e^{\mathrm{T}}\boldsymbol{\omega}_e}{\rho_2^2}\frac{2\rho_2\dot{\rho}_2\left(\rho_2^2 - \boldsymbol{\omega}_e^{\mathrm{T}}\boldsymbol{\omega}_e\right) - \rho_2^2\left(2\rho_2\dot{\rho}_2 - 2\boldsymbol{\omega}_e^{\mathrm{T}}\dot{\boldsymbol{\omega}}_e\right)}{\left(\rho_2^2 - \boldsymbol{\omega}_e^{\mathrm{T}}\boldsymbol{\omega}_e\right)^2} \\ &= \dot{V}_1 + \frac{-\dot{\rho}_2\boldsymbol{\omega}_e^{\mathrm{T}}\boldsymbol{\omega}_e + \rho_2\boldsymbol{\omega}_e^{\mathrm{T}}\dot{\boldsymbol{\omega}}_e}{\rho_2\left(\rho_2^2 - \boldsymbol{\omega}_e^{\mathrm{T}}\boldsymbol{\omega}_e\right)} \end{aligned} \tag{28}$$

By (3), one can obtain

$$\begin{aligned} \dot{\boldsymbol{\omega}}_e &= \dot{\boldsymbol{\omega}} - \dot{\boldsymbol{\omega}}_d \\ &= \boldsymbol{F}_\omega + \boldsymbol{g}_\omega\boldsymbol{u} - \dot{\boldsymbol{\omega}}_d \end{aligned} \tag{29}$$

Substituting (29) into (28) yields

$$\begin{aligned} \dot{V}_2 =& \dot{V}_1 + \frac{1}{\rho_2^2 - \boldsymbol{\omega}_e^{\mathrm{T}}\boldsymbol{\omega}_e}\left(-\frac{\dot{\rho}_2}{\rho_2}\boldsymbol{\omega}_e^{\mathrm{T}}\boldsymbol{\omega}_e + \boldsymbol{\omega}_e^{\mathrm{T}}\dot{\boldsymbol{\omega}}_e\right) \\ =& -\frac{K_1\boldsymbol{\Omega}_{\mathrm{e}}^{\mathrm{T}}\Omega_{\mathrm{e}}}{\rho_1^2 - \boldsymbol{\Omega}_{\mathrm{e}}^{\mathrm{T}}\boldsymbol{\Omega}_{\mathrm{e}}} + \frac{1}{\rho_2^2 - \boldsymbol{\omega}_e^{\mathrm{T}}\boldsymbol{\omega}_e}\left[-\frac{\dot{\rho}_2}{\rho_2}\boldsymbol{\omega}_e^{\mathrm{T}}\boldsymbol{\omega}_e + \boldsymbol{\omega}_e^{\mathrm{T}}(\boldsymbol{F}_\omega + \boldsymbol{g}_\omega\boldsymbol{u} - \dot{\boldsymbol{\omega}}_d)\right] \\ =& -\frac{K_1\boldsymbol{\Omega}_{\mathrm{e}}^{\mathrm{T}}\Omega_{\mathrm{e}}}{\rho_1^2 - \boldsymbol{\Omega}_{\mathrm{e}}^{\mathrm{T}}\boldsymbol{\Omega}_{\mathrm{e}}} + \frac{\boldsymbol{\omega}_e^{\mathrm{T}}}{\rho_2^2 - \boldsymbol{\omega}_e^{\mathrm{T}}\boldsymbol{\omega}_e}\left(-\frac{\dot{\rho}_2}{\rho_2}\boldsymbol{\omega}_e + \boldsymbol{F}_\omega + \boldsymbol{g}_\omega\boldsymbol{u} - \dot{\boldsymbol{\omega}}_d + \frac{1}{2}\frac{\boldsymbol{\omega}_e}{\rho_2^2 - \boldsymbol{\omega}_e^{\mathrm{T}}\boldsymbol{\omega}_e}\right) \\ &- \frac{1}{2}\frac{1}{(\rho_2^2 - \omega_e^{\mathrm{T}}\boldsymbol{\omega}_e)^2}\boldsymbol{\omega}_e^{\mathrm{T}}\boldsymbol{\omega}_e \end{aligned} \tag{30}$$

According to the conclusion derived from FXTESO above, in fixed time T, the FXTESO output $\boldsymbol{z}_{\mathbf{2}}$ converges to the total disturbances $\boldsymbol{F}_\omega$. Therefore, the controller is designed as follows:

$$\boldsymbol{u} = \boldsymbol{g}_\omega^{-\mathbf{1}}\left(-K_2\boldsymbol{\omega}_e + \frac{\dot{\rho}_2}{\rho_2}\boldsymbol{\omega}_e - \boldsymbol{z}_2 + \dot{\boldsymbol{\omega}}_d - \frac{1}{2}\frac{\boldsymbol{\omega}_e}{\rho_2^2 - \boldsymbol{\omega}_e^{\mathrm{T}}\boldsymbol{\omega}_e}\right) \tag{31}$$

where $K_2 = \mathrm{diag}(k_{21}, k_{22}, k_{23})$ is a positive definite matrix.

By invoking (31) into (30), it can be obtained that

$$\dot{V}_2 = -\frac{K_1\boldsymbol{\Omega}_{\mathrm{e}}^{\mathrm{T}}\Omega_{\mathrm{e}}}{\rho_1^2 - \boldsymbol{\Omega}_{\mathrm{e}}^{\mathrm{T}}\boldsymbol{\Omega}_{\mathrm{e}}} - \frac{K_2\boldsymbol{\omega}_{\mathrm{e}}^{\mathrm{T}}\omega_{\mathrm{e}}}{\rho_2^2 - \boldsymbol{\omega}_{\mathrm{e}}^{\mathrm{T}}\boldsymbol{\omega}_{\mathrm{e}}} + \frac{\boldsymbol{\omega}_e^{\mathrm{T}}\boldsymbol{e}_2}{\rho_2^2 - \boldsymbol{\omega}_e^{\mathrm{T}}\boldsymbol{\omega}_e} - \frac{1}{2}\frac{\boldsymbol{\omega}_e^{\mathrm{T}}\boldsymbol{\omega}_e}{(\rho_2^2 - \boldsymbol{\omega}_e^{\mathrm{T}}\boldsymbol{\omega}_e)^2} \tag{32}$$

Utilizing basic inequality, one has

$$\frac{\boldsymbol{\omega}_e^{\mathrm{T}}\boldsymbol{e}_2}{\rho_2^2 - \boldsymbol{\omega}_e^{\mathrm{T}}\boldsymbol{\omega}_e} \leqslant \frac{1}{2}\frac{\boldsymbol{\omega}_e^{\mathrm{T}}\boldsymbol{\omega}_e}{(\rho_2^2 - \boldsymbol{\omega}_e^{\mathrm{T}}\boldsymbol{\omega}_e)^2} + \frac{1}{2}\boldsymbol{e}_2^{\mathrm{T}}\mathbf{e}_2. \tag{33}$$

That is,

$$\dot{V}_2 \leqslant -\frac{k_1 \mathbf{\Omega}_e^T \Omega_e}{\rho_1^2 - \mathbf{\Omega}_e^T \mathbf{\Omega}_e} - \frac{k_2 \boldsymbol{\omega}_e^T \omega_e}{\rho_2^2 - \boldsymbol{\omega}_e^T \boldsymbol{\omega}_e} + \frac{1}{2} \boldsymbol{e}_2^T \mathbf{e}_2 \tag{34}$$

Design k_i as follows:

$$k_i = \min\{k_{ij}, j = 1,2,3\}, i = 1,2. \tag{35}$$

According to Theorem 1, the estimation error will converge to a small range, so $\|\boldsymbol{e_2}\|^2 \leqslant \zeta$.

$$\dot{V}_2 \leqslant -\frac{k_1 \mathbf{\Omega}_e^T \Omega_e}{\rho_1^2 - \mathbf{\Omega}_e^T \mathbf{\Omega}_e} - \frac{k_2 \boldsymbol{\omega}_e^T \omega_e}{\rho_2^2 - \boldsymbol{\omega}_e^T \boldsymbol{\omega}_e} + \xi, \tag{36}$$

where

$$\xi = \frac{\zeta}{2} > 0. \tag{37}$$

The barrier Lyapunov functions V_2 are organized as follows:

$$V_2 = \frac{1}{2} \ln \frac{\rho_1^2}{\rho_1^2 - \mathbf{\Omega}_e^T \mathbf{\Omega}_e} + \frac{1}{2} \ln \frac{\rho_2^2}{\rho_2^2 - \boldsymbol{\omega}_e^T \boldsymbol{\omega}_e}, \tag{38}$$

$$\dot{V}_2 \leqslant -\frac{k_1 \mathbf{\Omega}_e^T \Omega_e}{\rho_1^2 - \mathbf{\Omega}_e^T \mathbf{\Omega}_e} - \frac{k_2 \boldsymbol{\omega}_e^T \omega_e}{\rho_2^2 - \boldsymbol{\omega}_e^T \boldsymbol{\omega}_e} + \xi, \tag{39}$$

By Lemma 1, it follows that

$$\begin{aligned} \dot{V}_2 &\leqslant -k_1 \ln \frac{\rho_1^2}{\rho_1^2 - \mathbf{\Omega}_e^T \mathbf{\Omega}_e} - k_2 \ln \frac{\rho_2^2}{\rho_2^2 - \boldsymbol{\omega}^T \boldsymbol{\omega}} + \xi \\ &\leqslant -k V_2 + \xi, \end{aligned} \tag{40}$$

where $k = \min\{2k_i, i = 1,2\}$. It is obvious that $\dot{V}_2 < 0$ when $V_2 > \frac{\xi}{k}$.

Consequently, it follows from (40) that

$$V_2(t) \leqslant e^{-kt} V_2(0) + \frac{\xi}{k}\left(1 - e^{-kt}\right). \tag{41}$$

By (41), there holds

$$\lim_{t \to \infty} \sup V_2(t) \leqslant \frac{\xi}{k} \tag{42}$$

From the above analysis, it can be obtained:

$$\begin{aligned} &\lim_{t \to \infty} \sup \|\mathbf{\Omega}_e\| \leqslant \rho_{1\infty} \sqrt{1 - e^{-\frac{2\xi}{k}}}, \\ &\lim_{t \to \infty} \sup \|\boldsymbol{\omega}_e\| \leqslant \rho_{2\infty} \sqrt{1 - e^{-\frac{2\xi}{k}}} \end{aligned} \tag{43}$$

The attitude angles and attitude angular rates errors are constrained by ρ_1 and ρ_2, respectively.

A novel integration of FXTESO with PPC is proposed, ensuring that the state of the aircraft attitude control system is stabilized within a prescribed performance range and providing an important contribution to the fault-tolerant control strategy of the aircraft attitude.

Remark 2. *The BLF and PPC design method offers two benefits compared to other controllers. First, the PPC has a simpler structure than other controllers. Second, the PPC is unaffected by the chattering issue caused by the sign function or the singularity problem caused by fractional-order exponentials.*

4. Simulation and Analysis

The initial flight attitude is set to $\phi = 0°, \theta = 0°, \psi = 0°$. The desired attitude angles are $\phi_d = 1°, \theta_d = 1°, \psi_d = 1°$. The disturbances are designed as follows:

$$\boldsymbol{d}_\omega = \begin{bmatrix} d_1(t) \\ d_2(t) \\ d_3(t) \end{bmatrix} = \begin{bmatrix} 0.01\sin(0.5t) \\ 0.01\sin(t) \\ 0.01\cos(2t) \end{bmatrix} \tag{44}$$

The parameters of PPC are selected as

$$\begin{aligned} \rho_{10} = 0.087, \rho_{1\infty} = 0.0035, l_1 = 0.5 \\ \rho_{20} = 0.14, \rho_{2\infty} = 0.0087, l_2 = 0.5. \end{aligned}$$

The parameters of FXTESO are $\lambda_1 = 36, \lambda_2 = 432, k_1 = 36, k_2 = 432, a = 0.8, b = 1.2, K = 0.1$. λ_i and k_i (for $i = 1,2$) represent the observer gains. By increasing the gain of the fixed-time extended state observer, the convergence speed of the extended state observer can be made faster. The rest control parameters are given by $K_1 = \mathrm{diag}(1,1,1), K_2 = \mathrm{diag}(5,5,5)$.

A comparison with the finite-time extended state observer (FTESO) from the literature [25] is provided to demonstrate the accuracy and efficiency of the fixed-time extended state observer. The following is the formula for FTESO:

$$\begin{cases} \boldsymbol{e}_1 = \boldsymbol{z}_1 - \boldsymbol{x}_1 \\ \dot{\boldsymbol{z}}_1 = \boldsymbol{g}_\omega \boldsymbol{u} - \eta_1 \,\mathrm{sig}^{\beta_1}(\boldsymbol{e}_1) + \boldsymbol{z}_2 \\ \dot{\boldsymbol{z}}_2 = -\eta_2 \,\mathrm{sig}^{\beta_2}(\boldsymbol{e}_1) \end{cases} \tag{45}$$

Aircraft parameters are shown in Table 1.

Table 1. Aircraft parameters.

Meaning	Symbol	Value
Wing area	S	12.53 m^2
Wing span	b	8.016 m
Mean aerodynamic chord	c	1.645 m
Roll moment of inertia	J_x	1016.86 $\mathrm{kg}\cdot\mathrm{m}^2$
Pith moment of inertia	J_y	6236.76 $\mathrm{kg}\cdot\mathrm{m}^2$
Yaw moment of inertia	J_z	6779 $\mathrm{kg}\cdot\mathrm{m}^2$
Product moment of inertia	J_{xz}	271.16 $\mathrm{kg}\cdot\mathrm{m}^2$

Stability Comparison

The efficacy of PPC-FXTESO is verified through a comparison with the attitude tracking controller using the extended state observer-based backstepping control (BSC-ESO) approach. Figures 3 and 4 show the UAV tracking the desired attitude angle and attitude angle rate. The error responses of attitude angles and attitude angular rates, denoted as $\boldsymbol{e}_1$ and $\boldsymbol{e}_2$, are presented in Figures 5 and 6. Perturbations estimated by FXTESO are illustrated in Figure 7. Figure 8 compares estimation errors using FXTESO, FTESO, and ESO.

From Figures 3 and 4, and the comparison data in Table 2, it can be seen that the average settling time of PPC-FXTESO is 6.2 s. The average settling times of BSC-ESO and BSC-FTESO are 14.97 s and 12.56 s, respectively. Consequently, the proposed control scheme exhibits faster convergence to the desired attitude angle and attitude angle rate. When the actuator faults at 10 s, the attitude angles and attitude angular rates deviate but quickly stabilize and track the desired values. For instance, considering the tracking response of ϕ in Figure 3, although the maximum overshoot of the three methods is roughly identical, the convergence time when utilizing PPC-FXTESO is notably superior to that of BSC-ESO and BSC-FTESO. The response p indicates that the stabilization time of PPC and BSC is approximately 7.96 s and 13.3 s, respectively. From the data in Table 2, it can be seen that under the proposed control scheme, the overshoot and settling time of the attitude angle are smaller than the other two control schemes, so the PPC scheme has faster convergence, higher tracking accuracy, and better robustness to external disturbances.

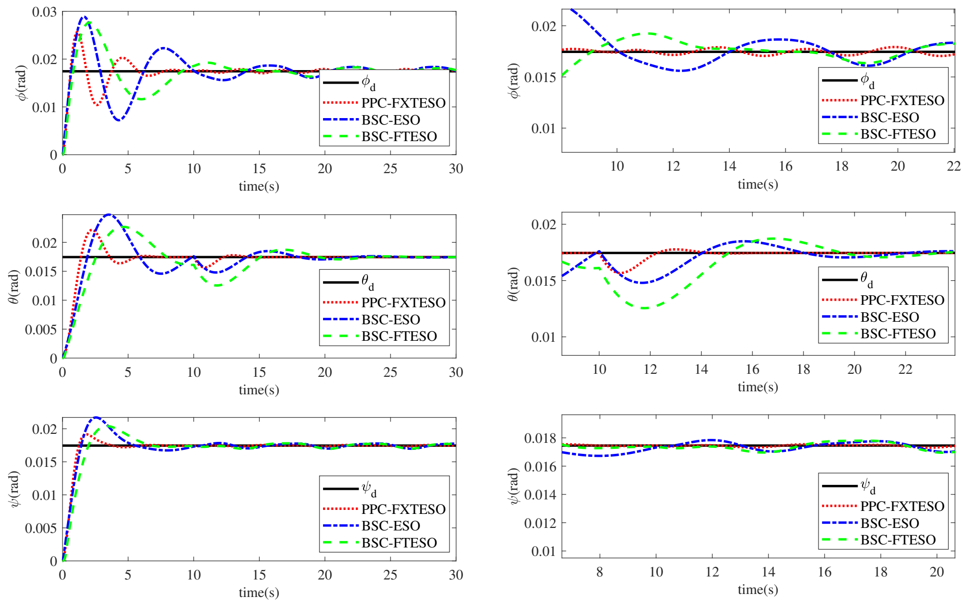

Figure 3. Attitude angle tracking and partial enlargement during actuator faults.

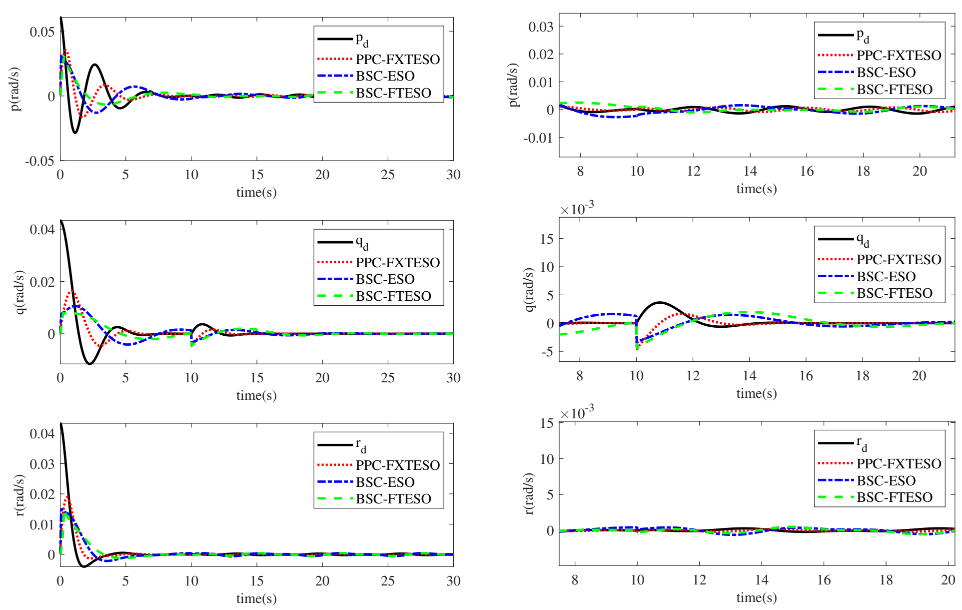

Figure 4. Attitude angular rates tracking and partial enlargement during actuator faults.

The tracking response of θ in Figure 5 shows that despite actuator faults, the tracking error of attitude angles consistently remains within the prescribed performance range. However, following the actuator failure at 10 s, the tracking error of the BSC-FTESO is 0.0049 rad, exceeding the prescribed performance range of 0.0035 rad, thus breaching the performance function boundary. The state error curve of BSC-ESO initially exceeds the performance function boundary. The above analysis indicates that under PPC-FXTESO, the state change is relatively gentle, and the convergence speed is fast, ensuring that the error consistently remains within a prescribed performance range, thus satisfying the system constraints.

Table 2. Comparison of attitude tracking overshoot and settling time.

Channels	PPC-FXTESO		BSC-FTESO		BSC-ESO	
	Overshoot	**Time**	**Overshoot**	**Time**	**Overshoot**	**Time**
ϕ	0.0085 rad	8.25 s	0.01 rad	13.45 s	0.0114 rad	14.17 s
θ	0.0047 rad	6.1 s	0.0052 rad	14.9 s	0.007 rad	17.87 s
ψ	0.002 rad	5 s	0.0029 rad	7.26 s	0.004 rad	14.9 s
p	0.0037 rad/s	7.96 s	0.082 rad/s	13.3 s	0.092 rad/s	14 s
q	0.0014 rad/s	5.37 s	0.04 rad/s	18 s	0.06 rad/s	19 s
r	0.007 rad/s	4.7 s	0.023 rad/s	8.5 s	0.033 rad/s	9.9 s

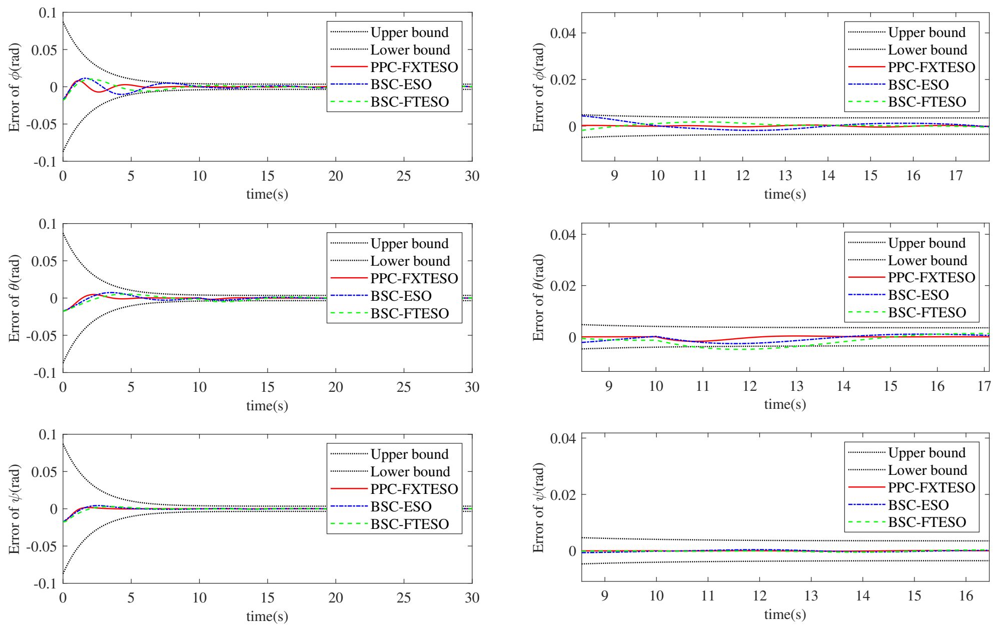

Figure 5. Attitude angle tracking error and partial enlargement during actuator faults.

For the attitude inner loop channel, Figure 7 depicts the total perturbation $f_i(i = 1, 2, 3)$ (continuous line), as well as its estimated value (dashed line) obtained through the fixed-time extended state observer; from the estimation point of view, FXTESO is convergent because the estimated perturbation $\hat{f}_i(i = 1, 2, 3)$ converges to its actual value. Figure 8 demonstrates the observer estimation error, and it can be seen that the estimation error of FXTESO remains stable. The estimation error fluctuates when the actuator fails at 10 s. Taking the estimation of f_2 as an example, the estimation error of ESO is 11.68, the estimation error of FTESO is 22, and the estimation error of FXTESO is 2.5. It is evident that when the UAV is disturbed by actuator faults, FXTESO exhibits the smallest estimation error, with its estimation error trending toward 0 within 3 s. In contrast, ESO and FTESO estimation errors converge at 13 s and 12 s, respectively. The results show that the fixed-time observer has better estimation capability.

The actuator deflections are shown in Figure 9. When the actuator fails at 10 s, the elevator rudder of PPC-FXTESO experiences a 0.12 rad deflection and stabilizes within 5 s. In contrast, BSC-FTESO and BSC-ESO stabilize after 10 s. During the UAV tracking of the desired attitude, the stabilization times for the aileron and rudder with PPC-FXTESO are 9 s and 7 s, while with BSC-FTESO, they are 12 s and 13 s, respectively. Hence, the actuator deflection with the proposed method tends to stabilize more quickly.

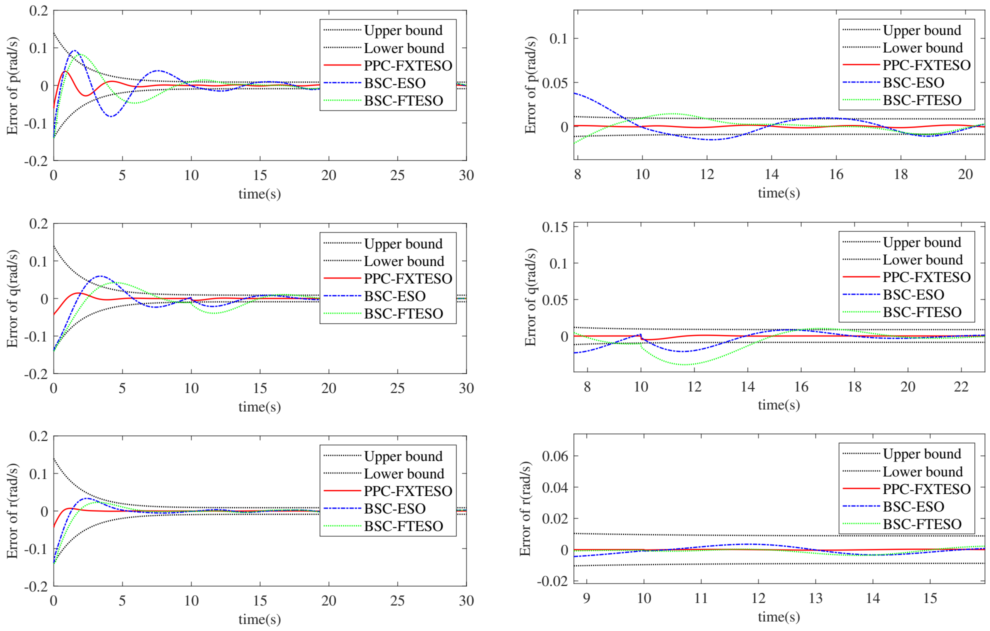

Figure 6. Attitude angular rates tracking error and partial enlargement during actuator faults.

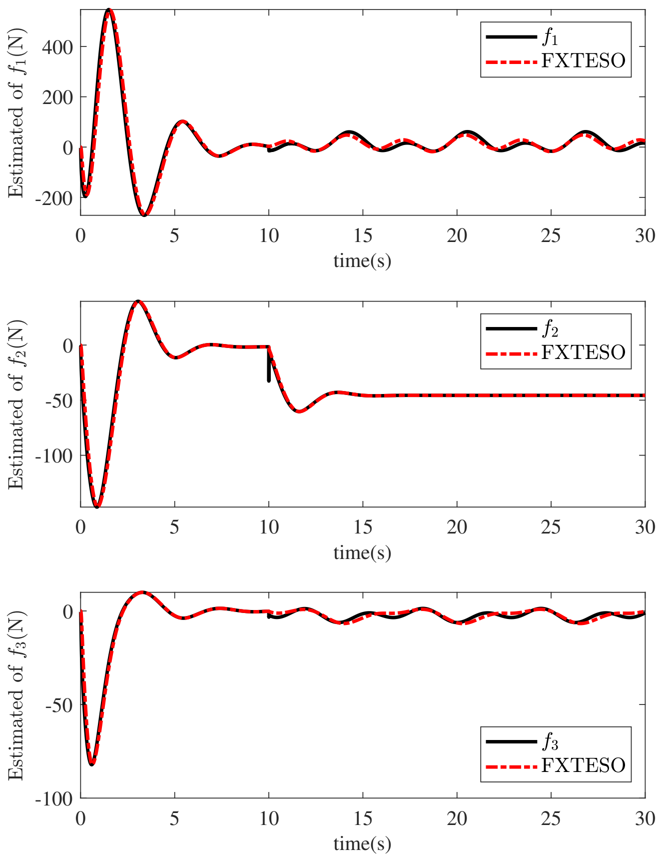

Figure 7. Lumped disturbance estimation for attitude control systems.

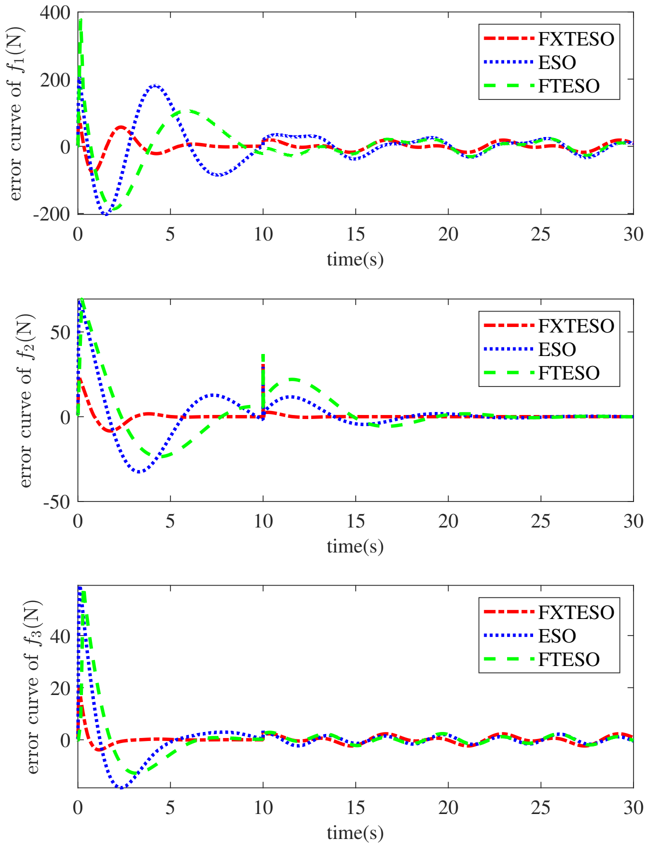

Figure 8. Observer estimation error curve.

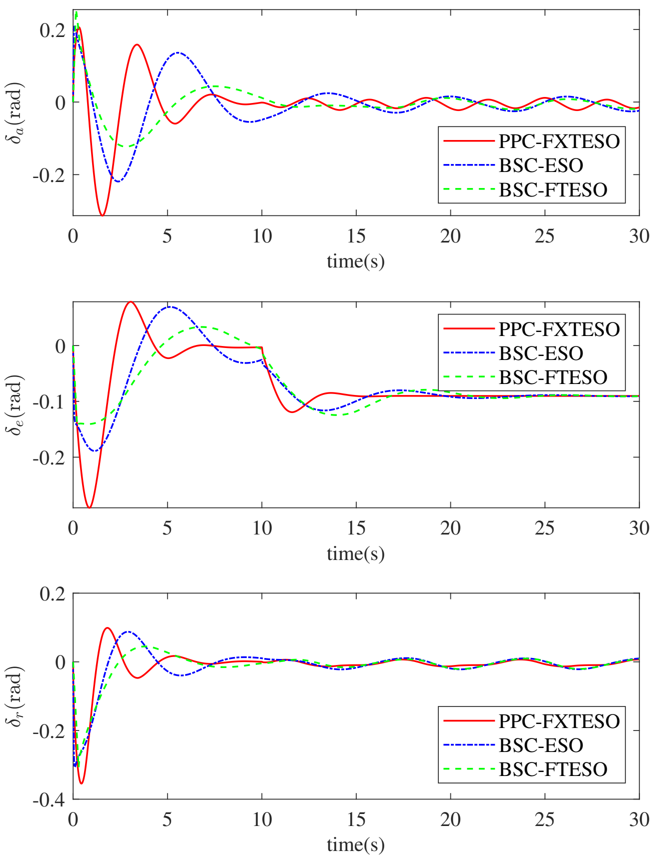

Figure 9. Actuators deflection.

5. Conclusions

The prescribed performance controller is designed for the attitude tracking control problem of the carrier-based UAV with actuator faults. For the tracking error performance constraint, a performance function is designed that utilizes the barrier Lyapunov function to ensure that the state of the attitude system is constrained to be within the interval even if the actuator faults. For systems with time-varying disturbances, the proposed FXTESO is designed to estimate the total disturbances in the system, which has a greater convergence speed and convergence accuracy than conventional extended state observers. The simulation results show that the controller has the advantages of high tracking accuracy, fault tolerance, and strong anti-interference ability. However, it also comes with computational requirements and control parameter tuning challenges. Careful consideration of these factors is essential in determining the suitability and feasibility of adopting this control approach for UAV applications.

Author Contributions: Conceptualization, Q.Z. and Q.W.; methodology, Q.Z. and Q.W.; software, Q.W.; validation, Q.Z. and Q.W.; formal analysis, Q.Z. and Q.W.; resources, Q.Z.; writing and editing, Q.W.; review, Q.Z.; visualization, Q.Z. and Q.W.; supervision, Q.Z.; funding acquisition, Q.Z. All authors have read and agreed to the published version of the manuscript.

Funding: This research was funded by the National Natural Science Foundation of China (Grant Number 52171299).

Data Availability Statement: The data that support the findings of this study are available on request from the corresponding author, upon reasonable request, and with the permission of the laboratory confidentiality agency.

Conflicts of Interest: The authors declare no conflicts of interest.

References

1. Emami, S.A.; Banazadeh, A. Online identification of aircraft dynamics in the presence of actuator faults. *J. Intell. Robot. Syst.* **2019**, *96*, 541–553. [CrossRef]
2. Liu, Y.; Dong, X.; Ren, Z.; Cooper, J. Fault-tolerant control for commercial aircraft with actuator faults and constraints. *J. Frankl. Inst.* **2019**, *356*, 3849–3868. [CrossRef]
3. Zhang, Y.; Liu, J.; He, W. Adaptive fault-tolerant control for a nonlinear flexible aircraft wing system. *Asian J. Control* **2019**, *21*, 2340–2351. [CrossRef]
4. Rudin, K.; Ducard, G.J.; Siegwart, R.Y. Active fault-tolerant control with imperfect fault detection information: Applications to UAVs. *IEEE Trans. Aerosp. Electron. Syst.* **2019**, *56*, 2792–2805. [CrossRef]
5. Yan, K.; Wu, Q.; Yang, C.; Chen, M. Backstepping-based Adaptive Fault-Tolerant Control Design for Satellite Attitude System. In Proceedings of the 2020 International Conference on Unmanned Aircraft Systems (ICUAS), Athens, Greece, 1–4 September 2020; pp. 176–181.
6. Jiang, Y.; Hu, Q.; Ma, G. Adaptive backstepping fault-tolerant control for flexible spacecraft with unknown bounded disturbances and actuator failures. *ISA Trans.* **2010**, *49*, 57–69. [CrossRef]
7. Shen, Q.; Yue, C.; Goh, C.H.; Wang, D. Active fault-tolerant control system design for spacecraft attitude maneuvers with actuator saturation and faults. *IEEE Trans. Ind. Electron.* **2018**, *66*, 3763–3772. [CrossRef]
8. Huo, J.; Meng, T.; Jin, Z. Adaptive Backstepping Sliding Mode Fault Tolerant Control for Satellite Attitude under Actuator Faults. In *IOP Conference Series: Materials Science and Engineering*; IOP Publishing: Bristol, UK, 2019; Volume 608, p. 012040.
9. Guo, F.; Lu, P. Improved adaptive integral-sliding-mode fault-tolerant control for hypersonic vehicle with actuator fault. *IEEE Access* **2021**, *9*, 46143–46151. [CrossRef]
10. Du, Y.; Huang, P.; Cheng, Y.; Fan, Y.; Yuan, Y. Fault tolerant control of a quadrotor unmanned aerial vehicle based on active disturbance rejection control and two-stage Kalman filter. *IEEE Access* **2023**, *11*, 67556–67566. [CrossRef]
11. Jung, W.; Bang, H. Fault and failure tolerant model predictive control of quadrotor UAV. *Int. J. Aeronaut. Space Sci.* **2021**, *22*, 663–675. [CrossRef]
12. Hu, C.; Cao, L.; Zhou, X.; Sun, B.; Wang, N. Fuzzy adaptive nonlinear sensor-fault tolerant control for a quadrotor unmanned aerial vehicle. *Asian J. Control* **2020**, *22*, 1163–1176. [CrossRef]
13. Nian, X.; Chen, W.; Chu, X.; Xu, Z. Robust adaptive fault estimation and fault tolerant control for quadrotor attitude systems. *Int. J. Control* **2020**, *93*, 725–737. [CrossRef]
14. Gómez-Peñate, S.; López-Estrada, F.R.; Valencia-Palomo, G.; Rotondo, D.; Guerrero-Sánchez, M.E. Actuator and sensor fault estimation based on a proportional multiple-integral sliding mode observer for linear parameter varying systems with inexact scheduling parameters. *Int. J. Robust Nonlinear Control* **2021**, *31*, 8420–8441. [CrossRef]

15. Guzman, J.; López-Estrada, F.R.; Estrada-Manzo, V.; Valencia-Palomo, G. Actuator fault estimation based on a proportional-integral observer with nonquadratic Lyapunov functions. *Int. J. Syst. Sci.* **2021**, *52*, 1938–1951. [CrossRef]
16. Gong, L.G.; Wang, Q.; Dong, C.Y. Spacecraft output feedback attitude control based on extended state observer and adaptive dynamic programming. *J. Frankl. Inst.* **2019**, *356*, 4971–5000. [CrossRef]
17. Ma, X.; Liu, S.; Cheng, H. Civil aircraft fault tolerant attitude tracking based on extended state observers and nonlinear dynamic inversion. *J. Syst. Eng. Electron.* **2022**, *33*, 180–187. [CrossRef]
18. Tang, P.; Lin, D.; Zheng, D.; Fan, S.; Ye, J. Observer based finite-time fault tolerant quadrotor attitude control with actuator faults. *Aerosp. Sci. Technol.* **2020**, *104*, 105968. [CrossRef]
19. Wu, X.; Luo, S.; Wei, C.; Liao, Y. Observer-based fault-tolerant attitude tracking control for rigid spacecraft with actuator saturation and faults. *Acta Astronaut.* **2021**, *178*, 824–834. [CrossRef]
20. Shao, X.; Wang, L.; Li, J.; Liu, J. High-order ESO based output feedback dynamic surface control for quadrotors under position constraints and uncertainties. *Aerosp. Sci. Technol.* **2019**, *89*, 288–298. [CrossRef]
21. Polyakov, A. Nonlinear feedback design for fixed-time stabilization of linear control systems. *IEEE Trans. Autom. Control* **2011**, *57*, 2106–2110. [CrossRef]
22. Zuo, Z.; Tie, L. Nonsingular fixed-time consensus tracking for second-order multi-agent networks. *Int. J. Control* **2014**, *87*, 363–370. [CrossRef]
23. Zuo, Z. Nonsingular fixed-time consensus tracking for second-order multi-agent networks. *Automatica* **2015**, *54*, 305–309. [CrossRef]
24. Ni, J.; Liu, L.; Liu, C.; Hu, X.; Li, S. Robust adaptive control of feedback linearizable MIMO nonlinear systems with prescribed performance. *IEEE Trans. Circuits Syst. II Express Briefs* **2016**, *64*, 151–155.
25. Zhao, J.; Feng, D.; Cui, J.; Wang, X. Finite-time extended state observer-based fixed-time attitude control for hypersonic vehicles. *Mathematics* **2022**, *10*, 3162. [CrossRef]
26. Bechlioulis, C.P.; Rovithakis, G.A. Robust adaptive control of feedback linearizable MIMO nonlinear systems with prescribed performance. *IEEE Trans. Autom. Control* **2008**, *53*, 2090–2099. [CrossRef]
27. Gao, S.; Liu, X.; Jing, Y.; Dimirovski, G.M. Finite-time prescribed performance control for spacecraft attitude tracking. *IEEE/ASME Trans. Mechatron.* **2021**, *27*, 3087–3098. [CrossRef]
28. Li, J.; Zhang, G.; Cabecinhas, D.; Pascoal, A.; Zhang, W. Prescribed performance path following control of USVs via an output-based threshold rule. *IEEE Trans. Veh. Technol.* **2023**, *73*, 6171–6182.
29. Guan, Z.; Ma, Y.; Zheng, Z.; Guo, N. Prescribed performance control for automatic carrier landing with disturbance. *Nonlinear Dyn.* **2018**, *94*, 1335–1349. [CrossRef]
30. He, M.; Rong, T.; Li, J.; He, C. Adaptive dynamic surface full state constraints control for stochastic Markov jump systems based on event-triggered strategy. *Appl. Math. Comput.* **2021**, *392*, 125563. [CrossRef]
31. Lin, Y.; Zhuang, G.; Sun, W.; Zhao, J.; Chu, Y. Resilient H∞ dynamic output feedback controller design for USJSs with time-varying delays. *Appl. Math. Comput.* **2021**, *395*, 125875.
32. Tee, K.P.; Ge, S.S.; Tay, E.H. Barrier Lyapunov functions for the control of output-constrained nonlinear systems. *Automatica* **2009**, *45*, 918–927. [CrossRef]
33. Li, D.P.; Liu, Y.J.; Tong, S.; Chen, C.P.; Li, D.J. Neural networks-based adaptive control for nonlinear state constrained systems with input delay. *IEEE Trans. Cybern.* **2018**, *49*, 1249–1258. [CrossRef]
34. Shao, X.; Hu, Q.; Shi, Y.; Jiang, B. Fault-tolerant prescribed performance attitude tracking control for spacecraft under input saturation. *IEEE Trans. Control Syst. Technol.* **2018**, *28*, 574–582. [CrossRef]
35. Mohammadi, A.; Ramezani, A. A robust model predictive control-based method for fault detection and fault tolerant control of quadrotor UAV. *Trans. Inst. Meas. Control* **2023**, *45*, 37–48. [CrossRef]
36. Xiao, H.; Zhen, Z.; Xue, Y. Fault-tolerant attitude tracking control for carrier-based aircraft using RBFNN-based adaptive second-order sliding mode control. *Aerosp. Sci. Technol.* **2023**, *139*, 108408. [CrossRef]
37. Xu, Y.H.; Liu, X.; Zhou, W.; Yu, G. Generative adversarial LSTM networks learning for resource allocation in UAV-served M2M communications. *IEEE Wirel. Commun. Lett.* **2021**, *10*, 1601–1605. [CrossRef]
38. Sun, Q.; Yan, Y.; Xu, Y.; Yu, J. Multidimensional-Taylor-network-based robust optimal tracking control for MIMO nonlinear discrete-time systems. *ISA Trans.* **2023**, *142*, 606–614. [CrossRef] [PubMed]
39. Zheng, F.; Zhen, Z.; Gong, H. Observer-based backstepping longitudinal control for carrier-based UAV with actuator faults. *J. Syst. Eng. Electron.* **2017**, *28*, 322–377.
40. Yao, Z.; Kan, Z.; Zhen, C.; Shao, H.; Li, D. Fault-Tolerant control for carrier-based UAV based on sliding mode method. *Drones* **2023**, *7*, 194. [CrossRef]
41. Xue, Y.; Zhen, Z.; Yang, L.; Wen, L. Adaptive fault-tolerant control for carrier-based UAV with actuator failures. *Aerosp. Sci. Technol.* **2020**, *107*, 106227. [CrossRef]
42. Zhang, Y.; Wang, S.h.; Chang, B.; Wu, W.h. Adaptive constrained backstepping controller with prescribed performance methodology for carrier-based UAV. *Aerosp. Sci. Technol.* **2019**, *92*, 55–65. [CrossRef]
43. Denham, J.W. Project MAGIC CARPET: "Advanced controls and displays for precision carrier landings. In Proceedings of the 54th AIAA Aerospace Sciences Meeting, San Diego, CA, USA, 4–8 January 2016; p. 1770.
44. Han, J. From PID to active disturbance rejection control. *IEEE Trans. Ind. Electron.* **2009**, *56*, 900–906. [CrossRef]

45. Hu, Q.; Shao, X.; Guo, L. Adaptive fault-tolerant attitude tracking control of spacecraft with prescribed performance. *IEEE/ASME Trans. Mechatron.* **2017**, *23*, 331–341. [CrossRef]
46. Bhat, S.P.; Bernstein, D.S. Finite-time stability of continuous autonomous systems. *SIAM J. Control Optim.* **2000**, *38*, 751–766. [CrossRef]
47. Basin, M.; Yu, P.; Shtessel, Y. Finite-and fixed-time differentiators utilising HOSM techniques. *IET Control Theory Appl.* **2017**, *11*, 1144–1152. [CrossRef]